http://dx.doi.org/10.5012/bkcs.2012.33.9.2955

Matrix-Assisted Variable Wavelength Laser Desorption Ionization of Peptides; Influence of the Matrix Absorption Coefficient on Expansion Cooling

Sung Hee Ahn, Yong Jin Bae, and Myung Soo Kim*

*Department of Chemistry, Seoul National University, Seoul 151-742, Korea. *E-mail: myungsoo@snu.ac.kr*
Received May 1, 2012, Accepted June 11, 2012

Product ion yields in the in- and post-source decays of three peptide ions, $[Y_5X + H]^+$ (X = Y (tyrosine), K (lysine), and R (arginine)), generated by matrix-assisted laser desorption ionization (MALDI) were measured at six wavelengths, 307, 317, 327, 337, 347, and 357 nm, using α-cyano-4-hydroxycinnamic acid (CHCA) and 2,5-dihydroxybenzoic acid (DHB) as the matrices. The temperatures of the early and late plumes generated by MALDI were estimated *via* kinetic analysis of the product ion yield data. For both matrices, the temperature drop (ΔT), *i.e.* the difference in the temperature between the early and late plumes, displayed negative correlation with the absorption coefficient. This was in agreement with the previous reasoning that deeper laser penetration and larger amount of material ablation arising from smaller absorption coefficient would result in larger extent of expansion cooling. The results support the postulation of the expansion cooling occurring in the plume presented previously.

Key Words : Plume temperature, In-source decay, Post-source decay, Matrix absorption coefficient, Expansion cooling

Introduction

Matrix-assisted laser desorption ionization (MALDI)[1-5] is useful for mass spectrometry of labile biological molecules such as peptides and proteins. MALDI ion source is usually combined with a time-of-flight (TOF) analyzer even though other analyzers are also used.[6-8] Sequencing of peptide ions with MALDI-tandem TOF, which detects product ions generated from a selected precursor ion, is also useful in proteomics.[9,10]

A peptide ion generated by MALDI may dissociate spontaneously inside (in-source decay, ISD)[11,12] or outside (post-source decay, PSD)[13] the ion source and generate *b* and *y* type ions (see refs. 14 and 15 for the product ion notation). In addition to these *b*/*y* reactions,[16] a radical peptide cation may be formed *via* matrix ion-to-peptide ion hydrogen atom transfer. Recently, ISD after hydrogen atom transfer, that generates '*c*' and '*z*' type ions,[17,18] is attracting attention in relation to peptide and protein sequencing. In this work, however, we will focus on the *b*/*y* process in ISD of peptide ions – this will be shown to be dominant for small peptide ions investigated in this work. In the delayed extraction MALDI-TOF, ISD product ions generated before the application of the extraction pulse have the same kinetic energy as their precursor ions and hence form narrow fragment ion peaks in ordinary MALDI-TOF spectra.

Using a MALDI-TOF instrument equipped with an ion gate and a reflectron, it is possible to analyze the product ions generated in the region between the ion source exit and the reflectron entrance by spontaneous dissociation, *i.e.* PSD, of a selected precursor ion. When an apparatus equipped with a reflectron with constant electric field inside – this will be called L-reflectron because the potential is a linear function of the distance ($V = c_1x$, x is the distance from the reflectron entrance) – is tuned for a precursor ion, the time-focusing condition is not met for its PSD product ions. Then, low mass PSD product ions form a broad background instead of narrow peaks. Here, one way of improving the resolution is to record the spectra at several different reflectron voltages and stitch the results.[13] In a typical MALDI-TOF instrument, the flight time of a precursor ion from the ion source to the reflectron entrance is on the order of 10 μs.[19] Hence, this is the time scale for dissociation reactions observed by PSD. PSD spectra for peptide ions are almost completely dominated by *b*, *y*, and their consecutive dissociation products such as *a* (*b* - CO) and *z* (*y* - NH_3). A *z* type ion generated from *y* is different from those formed by radical ISD, which are mostly *z* + 1 and/or *z* + 2.[18]

ISD *via* *b*/*y* processes occurs efficiently, especially for peptide ions without any basic residue.[20,21] For example, we observed that 76% of $[Y_6 + H]^+$ (Y = tyrosine residue) dissociated *via* *b*/*y* ISD in MALDI with α-cyano-4-hydroxycinnamic acid (CHCA) as the matrix.[21] If the dissociation rate constant for $[Y_6 + H]^+$ remained constant inside the ion source, hardly any of the peptide ions would have survived by the time they arrived at the source exit. Then, the observation that some of them underwent PSD and that others even survived until they arrived at the detector meant that the rate constant decreased rapidly as the peptide ions moved from the sample plate to the source exit. Also observed was that ISD terminated rapidly, well within the minimum delay time of 150 ns used.[19] This was the reason why some peptide ions arrived at the detector in spite of its very efficient ISD. To find an explanation for this interesting observation, we estimated the effective temperatures of the peptide ion by kinetic analysis of its dissociation yields in

ISD and PSD.[19,21] The temperatures of the early and late CHCA plumes thus estimated were 874 and 461 K, respectively.[21] A large difference in the peptide ion temperature between the early and late plumes might occur if the ion activation mechanisms responsible for ISD and PSD are different, such as the exothermicity in proton transfer[17] for ISD and low-energy collisional activation for PSD.[1] However, a study utilizing UV-MALDI with a few matrices and IR-MALDI with glycerol showed that such an explanation was invalid.[21] As an alternative, we suggested that hot $[Y_6 + H]^+$ in the early matrix plume cooled as the plume expanded.[19,21]

A few cooling processes were suggested to occur in MALDI. An example is the evaporation cooling that would occur when a molecule leaves a condensed phase.[4] Such a process is irrelevant to the cooling in the gas-phase plume that we observed. The most likely explanation for the cooling in the plume is the expansion cooling that occurs upon the adiabatic expansion of a high density gas to the vacuum. In fact, the occurrence of the expansion cooling in MALDI was investigated theoretically and experimentally. Vertes and coworkers carried out hydrodynamic analysis for the matrix-assisted laser desorption of large molecules and concluded that a dramatic expansion cooling could occur.[22] Experimentally, occurrence of expansion cooling was inferred from supersonic 'initial' ion speeds (440-1400 ms^{-1})[3,23] and was proposed to stabilize labile analyte ions.[1,3,24]

To explain different amounts of the internal energy for the same peptide ion generated by MALDI with different matrices, Hillenkamp and Karas proposed to classify matrices as 'hard' or 'soft' presumably with a connotation that a harder matrix must be heated to a higher temperature for ablation because of its higher mechanical hardness and, hence, generates hotter plume.[1] Hillenkamp and Karas also noted that a harder matrix correlated with a lower initial ion speed and hence less expansion cooling.[1] We noted[21] that the mechanical hardness of a matrix crystal might not be the only factor affecting the plume temperature because IR-MALDI was invariably softer than UV-MALDI even when the same matrix was used for both.[25] Accordingly, the absorption coefficient at the MALDI laser wavelength was suggested as another factor that might affect the plume temperature. With a smaller absorption coefficient, the laser penetrates deeper, requiring larger energy for ablation. This would result in more material ablation, leading to more extensive expansion cooling. The two criteria for the matrix hardness, the mechanical hardness and the absorption coefficient, provided qualitative explanations for the temperature order for a peptide ion generated by MALDI with four matrices, *i.e.* CHCA, 2,5-dihydroxybenzoic acid (DHB), sinapinic acid (SA), and glycerol.[21]

In this work, the effective temperatures of some peptide ions in the early and late plumes of CHCA and DHB were determined at several MALDI laser wavelengths. Validity of the second criterion, *i.e.* a smaller absorption coefficient resulting in more extensive temperature drop, will be demonstrated.

Experimental

Details of the homebuilt MALDI-tandem TOF instrument used in this work were reported previously.[26-28] Briefly, it consists of an ion source with delayed extraction, a linear TOF analyzer, an ion gate, a PD cell (not used in this work), and a second-stage analyzer equipped with a reflectron with linear-plus-quadratic (LPQ, $V = c_1x + c_2x^2$) potential inside. A deflection system is installed inside the linear TOF.[27] This eliminates product ions generated by the dissociation of a precursor ion occurring between the ion source and the end of the system. Hence, only the product ions formed in the region between the end of this system and the reflectron entrance, which will be called the PSD region, appear in a PSD spectrum. The flight time of a precursor ion in the PSD region was 16.5% of its total flight time to the detector. A commercial MALDI-TOF instrument (UltrafleXtreme, Bruker Daltonics, Billerica, MA) was also used to record spectra.

Output of a dye laser (ND6000, Continuum, Santa Clara, CA) pumped by a Nd:YAG laser (PL8010, Continuum, Santa Clara, CA) was frequency-doubled to generate MALDI laser at 307 (rhodamine 101 dye), 317 (DCM), 327 (DCM), 337 (DCM + pyridine 1), 347 (pyridine 1), and 357 nm (pyridine 1 + pyridine 2). The laser beam with 5 mm diameter was focused by a lens with 250 mm focal length. For ease of controlling the fluence (laser pulse energy ÷ spot area), the distance between the lens and the sample plate was adjusted such that the spot diameter at the sample position became 180 μm regardless of the laser wavelength. For each set of peptide, matrix, and laser wavelength, the threshold pulse energy for MALDI was determined as the pulse energy at which a peptide ion and/or its product ion signals appear in 50% of MALDI shots.[19] Two times the threshold pulse energy was used in most of the measurements.

Peaks Appearing in a MALDI Spectrum. In MALDI-TOF of a peptide, several types of peptide-derived ions arrive at the detector. They are the peptide ion, its ISD and PSD product ions, and the PSD products of each ISD product. In the introductory section, we mentioned that ISD product ions appear as narrow peaks in a MALDI-TOF spectrum. In contrast, low mass PSD product ions form a broad background in a spectrum obtained with MALDI-TOF equipped with an L-reflectron. This necessitates voltage stepping in such instruments.[13] Previously, we showed that the resolution for low mass PSD product ions improved when a quadratic potential (c_2x^2) was added to the linear one (c_1x).[26,29] That is, not only the ISD products from a peptide ion but also its PSD product ions formed narrow peaks in an ordinary MALDI-TOF spectrum. As in conventional PSD operation, the precursor ion to each PSD product ion can be identified by activating the ion gate. It is to be noted that the flight time of a particular PSD ion is different from that of the same ion generated by ISD because their kinetic energies are different. In fact, all the ions in a MALDI-TOF spectrum can be identified by using two different mass calibration, one for the precursor ion and its ISD products and the other for PSD. Somewhat different resolving powers for ISD

(around 5000) and PSD (around 5000 near the precursor ion mass and unit mass resolution at *m/z* 100) peaks also help to distinguish these peaks. Capability to form narrow peaks for all types of ions is an important advantage for an LPQ instrument. This ensures the same experimental condition for their measurements.

Samples. The peptides YYYYYY (Y_6), angiotensin II (DRVYIHPF), and the matrices CHCA and DHB were purchased from Sigma (St. Louis, MO) and Y_5X (X = K and R) from Peptron (Daejeon, Korea). A matrix solution prepared with 1:1 acetonitrile/0.1% trifluoroacetic acid was mixed with aqueous solution of a peptide to get a sample solution with the matrix-to-peptide molar ratio of 1000:1. 1 μL of the solution containing 25 pmol of a peptide was loaded on the sample plate and vacuum-dried.

Results and Discussion

Laser Pulse Energy. The threshold laser pulse energy for each combination of peptide, matrix, and laser wavelength was measured following the guideline presented in the previous section. The threshold pulse energies thus determined are shown in Table 1. They were the same regardless of the peptides as far as the matrix and the laser wavelength were the same. The threshold pulse energy of 1.22 μJ/pulse for CHCA at 337 nm measured in this work was substantially larger than 0.75 μJ/pulse reported previously[19] because the laser spot size used in this work was larger.

From Beer's law, the equation relating the energy density (E/V) at the sample surface with the matrix absorption coefficient (a) and the laser fluence at the surface (H_0) is derived as follows.[3]

$$E/V = \alpha H_0 \quad (1)$$

Let us assume that the minimum, or threshold, energy density needed for the laser-induced ablation of a solid matrix is the same regardless of the laser wavelength. Then, Eq. (1) suggests that the threshold fluence for MALDI will be inversely proportional to the absorption coefficient for very thin samples. The absorption coefficients of the solid CHCA and DHB in the 307-357 nm range taken from ref. 30 are also listed in Table 1. The threshold pulse energy shows a decreasing trend as the absorption coefficient increases. A qualitative explanation is as follows. As the absorption coefficient of a matrix increases, the penetration depth of the laser decreases, depositing the photon energy in smaller volume. This results in smaller threshold pulse energy.

Previously, we suggested that a smaller absorption coefficient for a matrix would result in more material ablation, leading to more extensive expansion cooling.[21] One of the purposes of the present study was to estimate the temperatures in the early and late matrix plumes, and hence their differences, generated at different wavelengths. A question here was how much laser pulse energy – with the spot size fixed, fluence is proportional to pulse energy – we would use in MALDI at each wavelength. Based on Eq. (1), we assumed that the threshold pulse energy was a measure of the energy density in the irradiated sample. Then, to carry out experiments at the same energy density, we decided to use the same multiples of the threshold pulse energy regardless of the wavelength, two times the threshold pulse energy, to be specific.

Spectra. MALDI and PSD spectra of Y_5X (X = Y, K, and R) obtained at 337 nm with CHCA as the matrix were reported previously.[31] Even though MALDI and PSD spectra for Y_5K and Y_5R obtained with DHB as the matrix have not been reported, they are similar to the corresponding spectra obtained with CHCA except that product ions in DHB-MALDI are less abundant than in CHCA-MALDI. Product ions appearing in MALDI and PSD spectra obtained at wavelengths other than 337 nm were the same as those at 337 nm, even though their relative abundances were different. CHCA- and DHB-MALDI spectra of $[Y_5K + H]^+$ at 307 and 357 nm normalized to the precursor ion intensity are shown in Figure 1. As mentioned earlier, PSD product ions appear as narrow peaks in these spectra because the apparatus was equipped with an LPQ reflectron.[28] The PSD product ions were a_n (n = 2, 4, and 5), b_n (n = 2-5), y_n (n = 2-5), and the immonium Y. Similar product ions were generated by ISD also, as marked in the spectra. It is to be noted that the relative abundance of the immonium Y in ISD is much higher than in PSD. Higher temperature in the early plume seems to be responsible for the higher abundance of this ion generated by consecutive dissociations. Several PSD products of ISD fragments were identified. A few of them are marked in the spectra.

In the DHB-MALDI spectrum shown in Figure 1(c), c_n (n = 1-5), $z_n + 1$ (n = 2, 3, and 5), and $z_n + 2$ (n = 2, 3, and 5) also appear. The abundances of these ions generated *via* radical ISD are quite low compared to those for *b* and *y* type ions. In the case of Figure 1(c), the total abundance of the radical ISD product ions calculated after detector calibration was less than 5% of the corresponding value of the *b*/*y* ISD products. We hardly observed any radical ISD product ion in

Table 1. Absorption coefficients[a] of CHCA and DHB in the 307-357 nm spectral range and threshold laser pulse energies[b] for MALDI with CHCA and DHB

Matrix		307 nm	317 nm	327 nm	337 nm	347 nm	357 nm
CHCA	Absorption coefficient (10^4 cm^{-1})	9.6	13.0	17.3	21.8	26.9	31.2
	Threshold laser energy (μJ/pulse)	1.86 ± 0.15	1.59 ± 0.09	1.46 ± 0.12	1.22 ± 0.16	1.07 ± 0.15	0.88 ± 0.19
DHB	Absorption coefficient (10^4 cm^{-1})	5.1	6.0	7.1	8.0	8.4	8.7
	Threshold laser energy (μJ/pulse)	3.41 ± 0.22	3.11 ± 0.23	2.77 ± 0.24	2.55 ± 0.21	2.43 ± 0.20	2.39 ± 0.12

[a]Ref. 30. [b]Threshold pulse energies were essentially the same regardless of the peptides, Y_5X (X = Y, K, and R)

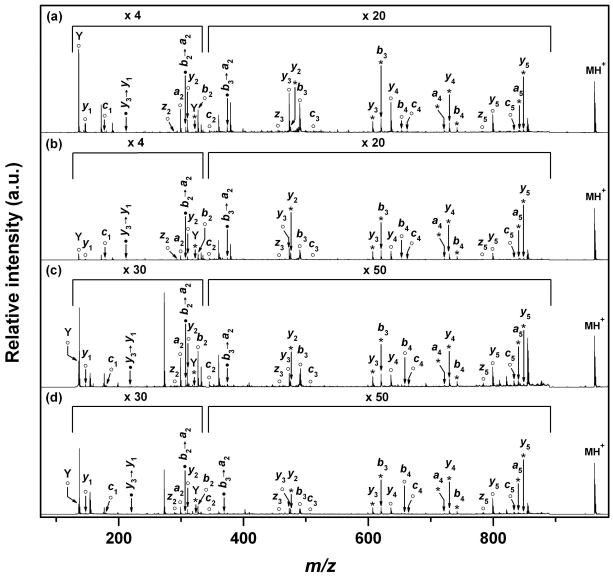

Figure 1. MALDI spectra of Y_5K. The matrix and the laser wavelength were (a) CHCA and 307 nm, (b) CHCA and 357 nm, (c) DHB and 307 nm, and (d) DHB and 357 nm. Each spectrum was obtained with laser pulse energy corresponding to two times the threshold determined under each condition and normalized to the precursor ion peak height. Prominent fragment ions formed by ISD (○), PSD (*), and PSD of ISD products (●) are marked. Other prominent peaks are due to the matrices.

CHCA-MALDI of Y_6. We also recorded DHB-MALDI spectra for Y_5K and Y_5R using a commercial instrument and observed a similar trend (Supporting Information). For angiotensin II, DRVYIHPF, the relative abundances of '*c*' and '*z*' ions tended to be higher than those for Y_5K and Y_5R, but still much lower than those for the *b*/*y* products (Supporting Information). For peptides containing a proline residue, Asakawa and Takayama[32] suggested that some *b* and *y* ions could be generated by complex dissociations after the hydrogen atom transfer. Based on the fact that the product ions generated by ISD are virtually the same as those by PSD and that proline residue is absent, we suggest that ISD of the two peptide ions studied in this work mostly occurs *via* the *b*/*y* channels.

Both in CHCA- and DHB-MALDI, the relative intensities of ISD peaks in MALDI at 307 nm are larger than at 357 nm, indicating higher early plume temperatures at 307 nm than at 357 nm. In contrast, the relative intensities of PSD peaks at the two wavelengths are rather similar, suggesting similar late plume temperatures. That is, the spectral patterns indicate larger temperature drop at 307 nm than at 357 nm.

Estimation of the Plume Temperatures. The kinetic method to estimate the temperatures of the early and late MALDI plumes was explained in details previously.[19,21] The method measures the product ion yields at the source exit and at the detector and analyzes them by utilizing the rate-energy relation, $k_{tot}(E)$, established for peptide ions in a previous kinetic study.[31] Briefly, each peak appearing in a time-of-flight spectrum, not a mass spectrum, was integrated over time and corrected for the detector gain to determine the number of ions in the peak. Even though the post-source dissociation of a precursor ion occurs over the entire region between the source exit and the detector, only those generated in a particular region, *i.e.* the PSD region, appear as PSD products. Since the time spent in the PSD region by a precursor ion was 16.5% of its total flight time, the number of ions in each PSD peak was multiplied by six – this correction factor did not significantly affected the final results.[19,31] Then, they were summed and normalized to the number of the precursor ion to get the total relative abundance for post-source dissociation, $Y_{total\ PSD}$. After making similar PSD correction for ISD peaks, they were summed and normalized to get the total relative abundance for in-source dissociation, $Y_{total\ ISD}$. The survival probabilities of the precursor ion at the source exit and at the detector, S_{in} and S_{post}, respectively, were estimated as $1/[1 + Y_{total\ ISD}]$ and $1/[1 + Y_{total\ PSD}]$. $Y_{total\ ISD}$, $Y_{total\ PSD}$, S_{in}, and S_{post} for $[Y_5X + H]^+$ (X = Y, K, and R) generated by MALDI at 307-357 nm are listed in Supporting Information.

Rice-Ramsperger-Kassel-Marcus (RRKM) rate constants, $k_{tot}(E)$, for the dissociation of $[Y_5X + H]^+$ were calculated using the critical energy (E_0) and entropy ($\Delta S^{\ddagger}$) reported previously,[31] *i.e.* E_0 = 0.600, 0.630, and 0.660 eV and $\Delta S^{\ddagger}$ = –28.4, –27.6, –27.2 eu (1 eu = 4.184 J mol^{-1} K^{-1}) for X = Y, K, and R, respectively. To estimate the early plume temperature, 50 ns was postulated as the lifetime of ISD,[19] or 1.4×10^7 s^{-1} in rate constant. For $[Y_5K + H]^+$, this corresponded to the rate constant at the internal energy (E) of 13.157 eV. Then, we made simplifying assumptions that the peptide ions were in thermal equilibrium in the early plume and that all the peptide ions with E > 13.157 eV underwent ISD. That is, the early plume temperature was determined such that the area under the internal energy distribution below 13.157 eV became equivalent to the experimental S_{in}. Similarly, the temperature in the late plume was determined by analyzing S_{post} with $k_{tot} = 5.5 \times 10^4$ s^{-1} as the threshold rate constant. The early (T_{early}) and late (T_{late}) plume temperatures of $[Y_5X + H]^+$ generated by CHCA- and DHB-MALDI at 307-357 nm are listed in Table 2 together with the early-to-late temperature drop (ΔT) in each case. ΔT was not determined for $[Y_5R + H]^+$ generated by DHB-MALDI because its ISD peaks were very weak and overlapped with matrix peaks. The errors quoted in the table are random ones determined by five or more replicate measurements for each.

Temperature Drop in Expansion Cooling. Before getting into the details of the temperature drops in expansion cooling, let us present a brief overview of our method to determine the temperatures. $[Y_6 + H]^+$ generated by CHCA-MALDI with two times the threshold pulse energy at 337 nm was one of the benchmarks in our study of the dissociation kinetics of peptide ions. E_0 of 0.60 eV and $\Delta S^{\ddagger}$ of –28.4 eu that specify its dissociation rate constant ($k_{tot}(E)$) were determined by time-resolved photodissociation.[33] This $k_{tot}(E)$ was used to estimate T_{early} and T_{late}, just as has been done in this work. Throughout the study, the internal energy of a peptide ion was assumed to display the thermal distribution at an effective temperature, which, in turn, was

Table 2. The effective temperatures (in K) in the early plume (T_{early}), late plume (T_{late}), and the temperature drop ($\Delta T = T_{early} - T_{late}$) in CHCA- and DHB-MALDI of Y_5X (X = Y, K, and R) at 307-357 nm

Matrix	Sample		307 nm	317 nm	327 nm	337 nm	347 nm	357 nm
CHCA	$[Y_6 + H]^+$	T_{early}	906 ± 5	895 ± 3	889 ± 5	878 ± 4	869 ± 5	863 ± 4
		T_{late}	454 ± 5	456 ± 2	456 ± 2	454 ± 2	452 ± 4	450 ± 3
		ΔT	452 ± 7	439 ± 3	433 ± 3	424 ± 5	417 ± 4	413 ± 5
	$[Y_5K + H]^+$	T_{early}	907 ± 5	898 ± 4	891 ± 2	880 ± 5	870 ± 7	859 ± 4
		T_{late}	458 ± 5	461 ± 3	459 ± 4	455 ± 2	450 ± 5	449 ± 2
		ΔT	449 ± 7	437 ± 6	432 ± 6	425 ± 3	420 ± 2	410 ± 3
	$[Y_5R + H]^+$	T_{early}	908 ± 8	901 ± 8	885 ± 3	881 ± 3	866 ± 7	861 ± 8
		T_{late}	460 ± 2	459 ± 2	456 ± 4	453 ± 6	447 ± 3	446 ± 6
		ΔT	448 ± 8	442 ± 8	429 ± 3	428 ± 3	419 ± 5	415 ± 3
DHB	$[Y_6 + H]^+$	T_{early}	843 ± 6	836 ± 3	826 ± 6	822 ± 4	823 ± 2	822 ± 6
		T_{late}	431 ± 3	427 ± 2	423 ± 2	422 ± 2	422 ± 1	426 ± 2
		ΔT	412 ± 3	409 ± 2	403 ± 6	400 ± 3	401 ± 2	396 ± 6
	$[Y_5K + H]^+$	T_{early}	844 ± 6	839 ± 3	831 ± 5	829 ± 4	826 ± 3	823 ± 4
		T_{late}	432 ± 3	429 ± 4	425 ± 2	426 ± 3	424 ± 1	424 ± 2
		ΔT	412 ± 3	410 ± 2	406 ± 6	403 ± 4	402 ± 2	399 ± 2

assumed to be unaffected by the presence of analytes that constituted 0.1% or less of a MALDI sample. Then, T_{early} and T_{late} determined for $[Y_6 + H]^+$ were used to determine E_0 and $\Delta S^{\ddagger}$ for the dissociation of other peptide ions such as $[Y_5K + H]^+$ and $[Y_5R + H]^+$ generated under the same MALDI condition.

One thing that might look remarkable about the temperature data in Table 2 is that T_{early}, T_{late}, and ΔT are unaffected by the identity of the peptide ion for which the measurement was made. For example, the temperatures of $[Y_6 + H]^+$, $[Y_5K + H]^+$, and $[Y_5R + H]^+$ in the early plume generated by CHCA-MALDI with two times the threshold at 307 nm are 906 ± 5, 907 ± 5, and 908 ± 8 K, respectively. This is not a real surprise considering that the method assumed the same temperature for different peptide ions in CHCA-MALDI at 337 nm. Still, it is a small surprise to note that the assumption held so well for MALDI by lasers with significantly different pulse energies at 307-357 nm and for two different matrices. In fact, the results are consistent with the thermal treatment of the processes occurring in MALDI.[4,21]

The temperature drops (ΔT) listed in Table 2 are drawn in Figure 2. For both of the matrices studied, the absorption coefficient increases with the wavelength as shown in Table 1, while ΔT decreases with the wavelength. Such a negative correlation between the absorption coefficient and ΔT was expected, but could not be quantitatively demonstrated until recently because no method was available to systematically estimate the plume temperature. Also to be noted from Table 2 is that the change in ΔT is larger with CHCA than with DHB in the 307-357 nm spectral range. This correlates well with the larger relative change in the absorption coefficient for CHCA in the same spectral range. The trend in ΔT *vs.* absorption cofficient data is in agreement with the qualitative reasoning that deeper laser penetration and larger amount of material ablation arising from smaller absorption coefficient result in larger extent of expansion cooling.

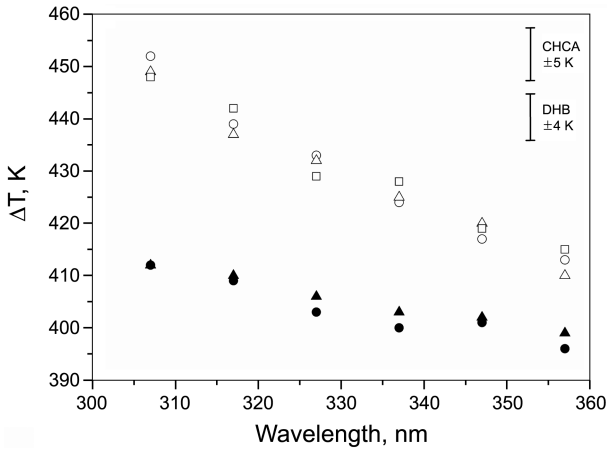

Figure 2. The temperature drop ($T = T_{early} - T_{late}$) *vs.* laser wavelength in MALDI. T data for Y_6, Y_5K, and Y_5R in CHCA-MALDI are denoted as open circles (○), open triangles (△), and open squares (□), respectively. Those for Y_6 and Y_5K in DHB-MALDI are denoted as filled circles (●) and filled triangles (▲), respectively. Typical error bars in CHCA- and DHB-MALDI results are also shown.

Based on Eq. (1), we assumed that the threshold pulse energy was a measure of the energy density in the irradiated sample. Hence, at each wavelength, we used two times the threshold pulse energy hoping to carry out measurements at the same energy density. Then, one might expect the same early plume temperature regardless of the wavelength. However, the data in Table 2 show that T_{early} decreases with the wavelength. We do not have an explanation for this trend. We would like to point out that Eq. (1) is the expression for the energy density at the sample surface after instantaneous absorption of radiation. In contrast, the ablation may also occur for molecules lying below the surface that would have lower energy. Also, the photo-activated surface molecules may undergo cooling *via* thermal conduction

before they ablate, that may affect the temperature of thin (large absorption coefficient) surface samples more than that of thick one.

Vibrational cooling in the adiabatic expansion of polyatomic molecules is an interesting subject in itself. Incomplete vibrational cooling of gas-phase polyatomic molecules generated by pulsed laser desorption was observed experimentally.[34] Theoretical description of the process is also under investigation.[35] At the moment, however, the phenomenon is not well understood enough to allow a reliable estimation of the extent of cooling. The data obtained in this work may be useful for the fundamental understanding of this phenomenon.

Conclusion

Even though many thermalizing collisions occur in the process of gas-phase ion formation from a peptide in MALDI, some ions survive 10 μs or longer while others undergo dissociation (ISD) within several tens of nanosecond. Previously, we estimated the temperatures of peptide ions in the early and late plumes and found that a substantial cooling occurred as the plume moved forward. We suggested that this occurred presumably *via* the adiabatic expansion of the high density early plume to the vacuum. We also suggested that the absorption coefficient of the matrix at the MALDI wavelength might be a factor affecting the temperature drop. Variable wavelength MALDI experiments carried out in this work supported the above prediction. More importantly, the results from the present study are compatible with and hence support the postulation of the expansion cooling occurring in the plume presented in a previous study.[21]

Acknowledgments. This work was supported by the National Research Foundation (NRF) grant funded by the Korea government (MEST) (20110030619). S. H. Ahn and Y. J. Bae thank the Ministry of Education, Science and Technology, Republic of Korea, for Brain Korea 21 Fellowship.

Supporting Information. 1. The total product ion abundances in the in- and post-source dissociations normalized to the precursor ion abundance, $Y_{\text{total ISD}}$ and $Y_{\text{total PSD}}$, respectively, for CHCA-MALDI of $[Y_5X + H]^+$ (X = Y, K, and R) and for DHB-MALDI of $[Y_5X + H]^+$ (X = Y and K) at 307-357 nm are listed in Table S1. The survival probability for a precursor ion at the source exit, S_{in}, estimated from $Y_{\text{total ISD}}$ and that at the detector, S_{post}, estimated from $Y_{\text{total PSD}}$ are also listed in the same table.

2. DHB-MALDI spectra of Y_5R, Y_5K, and angiotensin II recorded with a commercial instrument (UltrafleXtreme, Bruker Daltonics).

References

1. Hillenkamp, F.; Peter-Katalinić, J. *MALDI MS A Practical Guide to Instrumentation, Methods and Applications*; Wiley-VCH: Weinheim, Germany, 2007.
2. Zenobi, R.; Knochenmuss, R. *Mass Spectrom. Rev.* **1998**, *17*, 337-366.
3. Dreisewerd, K. *Chem. Rev.* **2003**, *103*, 395-425.
4. Knochenmuss, R. *Analyst.* **2006**, *131*, 966-986.
5. Dreisewerd, K.; Berkenkamp, S.; Leisner, A.; Rohlfing, A.; Menzel, C. *Int. J. Mass Spectrom.* **2003**, *226*, 189-209.
6. Zhang, W.; Krutchinsky, A. N.; Chait B. T. *J. Am. Soc. Mass Spectrom.* **2003**, *14*, 1012-1021.
7. Semmler, A.; Weber, R.; Przybylski, M.; Wittmann, V. *J. Am. Soc. Mass Spectrom.* **2010**, *21*, 215-219.
8. Strupat, K.; Kovtoun, V.; Bui, H.; Viner, R.; Stafford, G.; Horning, S. *J. Am. Soc. Mass Spectrom.* **2009**, *20*, 1451-1463.
9. Hernandez, P.; Müller, M.; Appel, R. D. *Mass Spectrom. Rev.* **2006**, *25*, 235-254.
10. Kinter, M.; Sherman, N. E. *Protein Sequencing and Identification Using Tandem Mass Spectrometry*; John Wiley: New York, U.S.A., 2000.
11. Brown, R. S.; Carr, B. L.; Lennon, J. J. *J. Am. Soc. Mass Spectrom.* **1996**, *7*, 225-232.
12. Köcher, T.; Engström, Å.; Zubarev, R. A. *Anal. Chem.* **2005**, *77*, 172-177.
13. Spengler, B. *J. Mass Spectrom.* **1997**, *32*, 1019-1036.
14. Roepstorff, P.; Fohlman, J. *J. Biomed. Mass Spectrom.* **1984**, *11*, 601.
15. Biemann, K. *Sequencing of Peptides by Tandem Mass Spectrometry and High-Energy Colision-Induced Dissociation. Methods in Enzymology*; Academic Press: New York, U.S.A., 1990.
16. Paizs, B.; Suhai, S. *Mass Spectrom. Rev.* **2005**, *24*, 508-548.
17. Demeure, K.; Gabelica, V.; De Pauw, E. A. *J. Am. Soc. Mass Spectrom.* **2010**, *21*, 1906-1917.
18. Takayama, M. *J. Am. Soc. Mass Spectrom.* **2001**, *12*, 1044-1049.
19. Yoon, S. H.; Moon, J. H.; Kim, M. S. *J. Am. Soc. Mass Spectrom.* **2010**, *21*, 1876-1883.
20. Sachon, E.; Clodic, G.; Blasco, T.; Jacquot, Y.; Bolbach, G. *Anal. Chem.* **2009**, *81*, 8986-8992.
21. Bae, Y. J.; Moon, J. H.; Kim, M. S. *J. Am. Soc. Mass Spectrom.* **2011**, *22*, 1070-1078.
22. Vertes, A.; Irinyi, G.; Gijbels, R. *Anal. Chem.* **1993**, *65*, 2389-2393.
23. Berkenkamp, S.; Menzel, C.; Hillenkamp, F.; Dreisewerd, K. *J. Am. Soc. Mass Spectrom.* **2002**, *13*, 209.
24. Glückmann, M.; Karas, M. *J. Mass Spectrom.* **1999**, *34*, 467-477.
25. Strupat, K.; Kampmeier, J.; Horneffer, V. *Int. J. Mass Spectrom. Ion Proc.* **1997**, *43*, 169-170.
26. Moon, J. H.; Yoon, S. H.; Kim, M. S. *Bull. Korean Chem. Soc.* **2005**, *26*, 763-768.
27. Yoon, S. H.; Moon, J. H.; Choi, K. M.; Kim, M. S. *Rapid Commun. Mass Spectrom.* **2006**, *20*, 2201-2208.
28. Bae, Y. J.; Yoon, S. H.; Moon, J. H.; Kim, M. S. *Bull. Korean Chem. Soc.* **2010**, *31*, 92-99.
29. Oh, J. Y.; Moon, J. H.; Kim, M. S. *J. Am. Soc. Mass Spectrom.* **2004**, *15*, 1248-1259.
30. Allwood, D. A.; Dreyfus, R. W.; Perera, I. K.; Dyer, P. E. *Rapid Commun. Mass Spectrom.* **1996**, *10*, 1575-1578.
31. Yoon, S. H.; Moon, J. H.; Kim, M. S. *J. Am. Soc. Mass Spectrom.* **2011**, *22*, 214-220.
32. Asakawa, D.; Takayama, M. *Rapid Commun. Mass Spectrom.* **2011**, *25*, 2379-2383.
33. Yoon, S. H.; Moon, J. H.; Kim, M. S. *J. Am. Soc. Mass Spectrom.* **2009**, *20*, 1522-1529.
34. Elam, J. W.; Levy, D. H. *J. Chem. Phys.* **1997**, *106*, 10368-10378.
35. Morozov, A. A. *Phys. Fluids* **2008**, *20*, 027103.